11Equation Section 1Criteria for Antibubble Formation from Drop Pairs Impinging on a Free Surface

Youngsup Song, Lenan Zhang, Evelyn N. Wang
Department of Mechanical Engineering, Massachusetts Institute of Technology, Cambridge, MA 02139, USA
Correspondence to: enwang@mit.edu

ABSTRACT

Antibubbles are fluid entities with the inverse phase of regular bubbles. While the structure and stability of antibubbles have been studied, a fundamental understanding of antibubble formation remains limited. We report a theoretical and experimental study of antibubble formation. In the experiment, pairs of surfactant-laden water drops impinged successively on the surface of the same liquid reservoir to create antibubbles. We propose four criteria for antibubble formation from a scaling analysis. Two dimensionless groups prescribe the likelihood of antibubble formation, the summative Weber number and the ratio of timescales between the capillarity driven pinch-off and the viscous drainage of air.

I. INTRODUCTION

An antibubble, the counterpart of an ordinary bubble, consists of a liquid drop separated from the bulk liquid by a thin film of gas (Fig. 1). Although relatively unfamiliar due to their ephemeral nature, antibubbles can be found in our daily lives; for example, when washing dishes or pouring beer into a glass [1,2]. Since first being reported in 1931 [3], antibubbles have been studied in a trickle of literature with several different names such as negative bubbles and inverted bubbles

[4,5] until the term “antibubble” was first coined in 1974 [1]. Recently, antibubble dynamics have sprung up again as an intriguing application of high-speed imaging. In particular, the fluid instability [6,7], collapse dynamics [8,9] and lifetime [10-13] of antibubbles have been extensively studied. The fundamental understanding of antibubble formation have, however, received relatively little attention. Although the formation process was explained qualitatively [7] and the optimal conditions for antibubble formation were studied statistically [14], physical insights into the interfacial interaction, fluid dynamics, and energy conversion responsible for antibubble formation remain not well-understood. In this work, the regime of antibubble formation by the impingement of drop pairs is characterized experimentally and leads to the development of a predictive theory. Our approach not only elucidates the formation criteria of antibubbles, but also provides useful guidelines to control antibubble generation.

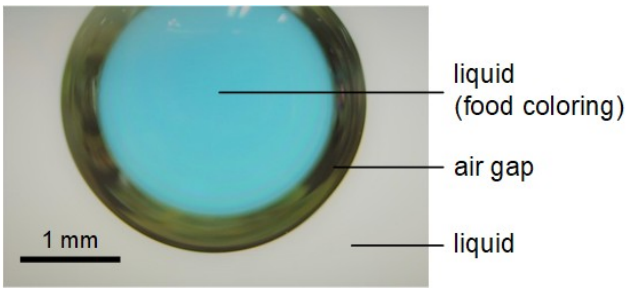

FIG. 1. Optical image of an antibubble separated from the bulk liquid by an air gap. Food-coloring was added in the antibubble to visually distinguish it from the bulk liquid.

II. EXPERIMENTAL

To understand the dynamic evolution of antibubble formation, we first performed experiments with the set-up shown in Fig. 2. A plexiglass container and a syringe were filled with a liquid

mixture of water and 1.0 wt% Triton X-100 surfactant (Dow Chemical Company), which has a surface tension σ = 30 dynes/cm = 0.030 N/m. The uncertainty of the surface tension of the mixture is negligible as the critical micellar concentration of the surfactant (0.1 wt%) is much less than the 1.0 wt% concentration used in this work. We used the surfactant for better stability and facile formation of antibubbles (See Supplemental Material I for details) [12,13,15-20]. The density ρ and the dynamic viscosity μ of the liquid mixture are approximately the same as that of water. To generate antibubbles, we first blocked the liquid reservoir by placing a lid over the bulk liquid and then started operating a syringe pump (PHD ULTRA 4400, Harvard Apparatus) with varying injection rates. Once the injection rate of syringe pump was stabilized, we removed the lid over the reservoir shortly to allow droplet impingement on the bulk liquid. We captured the first pair of drops that were impinged toward the quiescent surface of the bulk liquid using a high-speed camera (Phantom v7.1, Vision Research) with up to 4000 frames per second in order to study the dynamic evolution of the antibubble.

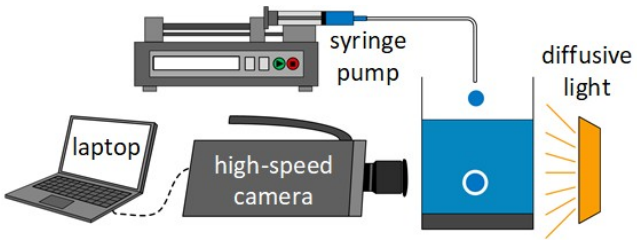

FIG. 2. Schematic of the experimental set-up. Surfactant-laden water drops impinge on the bulk liquid by a syringe pump to generate antibubbles. Antibubble formation process is captured by a high-speed camera

III. ANTIBUBBLE FORMATION CRITERIA

Fig. 3(a) shows schematics of the antibubble formation process by two impinging drops based on the experimental observation shown in Fig. 3(b). The overall formation process can be divided into four stages (Fig. 3). First, there are two drops successively approaching the surface. Second, the first drop coalesces with the bulk liquid and creates a surface deformation, into which the second drop impinges. In the third stage, the second drop further deforms the surface of bulk liquid, a thin air gap preventing its coalescence. In the fourth stage, the deformed surface pinches off due to surface tension, while a thin shell of air is trapped that separates the second drop from the bulk liquid. To understand this formation process, we considered the conversion of energy and the dynamics of pinch-off.

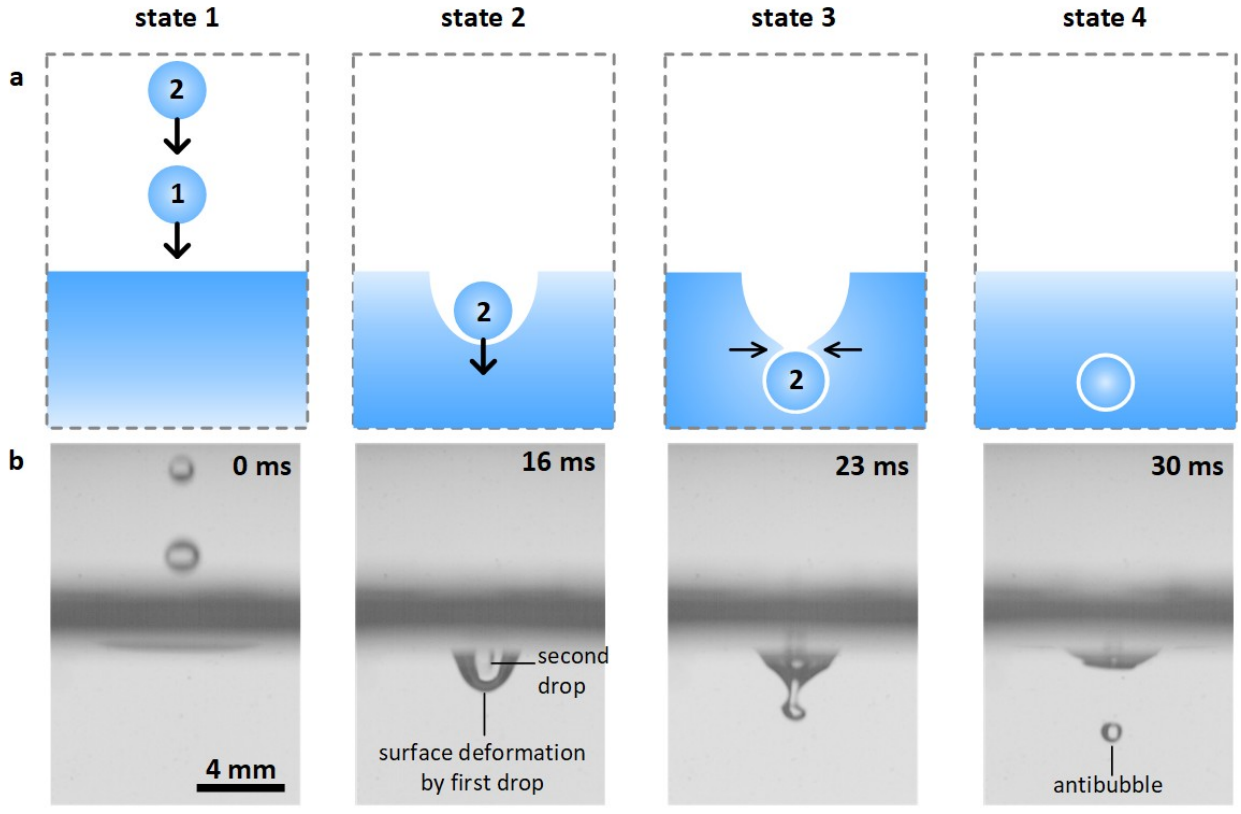

FIG. 3. Antibubble formation process. (a) Schematics and (b) corresponding experimental images in four states; two drops impinge onto the surface of reservoir successively (state 1), initial surface deformation by the first drop (state 2), further surface deformation by the second drop and pinch-off (state 3), leading to antibubble formation (state 4).

We first note that antibubbles can rarely be formed from a single drop impingement if the drop and the bulk are the same liquid in an isothermal condition, *i.e.*, both liquids with the same surface tension. Such a single drop impact on the bulk liquid has been extensively investigated, which can be classified into four regimes, *i.e.*, low-energy-coalescence, bouncing, high-energy-coalescence and jetting/splashing [19,21-30], where no regimes reported antibubble formation. An impinging drop with sufficiently high kinetic energy E_K for antibubble formation will eventually coalesce with the bulk surface according to the energy analysis (see Supplemental Material II for further discussion) [20]. Therefore, an antibubble formation from a single drop is infeasible. Alternatively, we consider the antibubble formation from a pair of drops in this work.

A. Initial surface deformation

For drop pairs impinging on the surface, we first consider the criterion required for the first impinging drop. The criterion can be extracted by analyzing the formation of state 2, where the first drop should create a crater-like initial surface deformation as shown in Fig. 3, so that the following drop can finally penetrate the surface and form an antibubble. To reach state 2, we consider the single drop impact with the bulk liquid, which can be classified in the four regimes as previously mentioned. The threshold of each regime can be characterized by the Weber

number $We = \rho u^2 d / \sigma$ and the Ohnesorge number $Oh = \mu / \sqrt{\rho \sigma d}$ of the impinging drop, where d and u are the diameter and velocity of an impinging drop, respectively. The crater-like surface deformation occurs in high-energy-coalescence and jetting/splashing regimes, which has been characterized by the experimental correlation [19,30],

$$We Oh^{-0.58} > 119. \qquad 22\text{* MERGEFORMAT ()}$$

Note that the jetting/splashing regime was excluded for both drops from our experiment and analysis due to practical considerations. In the jetting/splashing regime, a certain amount of the kinetic energy of the first impinging drop does not directly contribute to the crater-like surface deformation. Rather, the kinetic energy converts to the kinetic and surface energy of the liquid sheet or the secondary drops through viscous and surface forces. This effect makes the overall energy conversion analysis less straightforward (see Supplemental Material III for further discussion) [20,31-34].

B. Time-delay between two-drop impacts

The crater created by the coalescence of the first drop with the deep liquid pool initially expands due to inertia and then recedes under surface tension and gravity. In between, there is an instant that the crater reaches the maximum depth and the crater interface is stagnant, which means that the kinetic energy of the impinging drop is converted to the maximum available surface energy of the crater. This instant will be, therefore, optimal for the second drop impact. There have been extensive studies about the crater evolution from a drop impact onto a deep liquid pool [21-29]. In this section, we provide guidelines to find the optimal time-delay for an antibubble formation where the optimal time-delay can be determined by the impinging velocity u and droplet

diameter d. We numerically solved the crater evolution model from literature and compared it with our experimental data [26]. The crater can be modeled with a spherical shape as shown in Fig. 4(a).

The crater penetration depth z_{cr} can be expressed as the sum of the crater radius a and axial coordinate of the center of the sphere z_c, *i.e.*, $z_{cr} = a+z_c$. These three parameters are non-dimensionalized by scaling with the diameter of the drop d: dimensionless penetration depth Δ, crater radius α, and axial coordinate of the center of the sphere ζ, respectively. The crater evolution can be expressed by the second-order differential equations in terms of α and ζ for the inviscid flow outside the cavity when the impinging drop has diameter d and velocity u:

$$\ddot{\alpha} = -\frac{3}{2}\frac{\dot{\alpha}^2}{\alpha} - \frac{2}{\alpha^3 We} - \frac{1}{Fr}\frac{\zeta}{\alpha} + \frac{7}{4}\frac{\dot{\zeta}^2}{\alpha} \quad (33\text{* MERGEFORMAT ()})$$

$$\ddot{\zeta} = -3\frac{\dot{\alpha}\dot{\zeta}}{\alpha} - \frac{9}{2}\frac{\dot{\zeta}^2}{\alpha} - \frac{2}{Fr} \quad (44\text{* MERGEFORMAT ()})$$

where $Fr = u^2 / gd$ is the Froude number. We numerically solved the equations Error: Reference source not found and Error: Reference source not found. The resulting penetration depth as a function of time is plotted in Fig. 4(b) with our corresponding experimental data. The diameter and velocity of the impinging drop used in the plot are 2.48 mm and 1.24 m/s based on experimental measurement, respectively. The corresponding time-lapse snapshots from the high-speed camera are shown in Fig. 4(c). The model and experimental data show good agreement.

The optimal time-delay Δt_{opt} will occur when the crater is fully stretched, *e.g.*, ~15 ms in this

example. In Fig. 4(d), we plot the dimensionless optimal time-delay $\tau_{opt} = \Delta t_{opt}(u/d)$ as a function of the Weber number for different Froude numbers. The dimensional form of optimal time-delay is also shown as a function of the impinging velocity for different drop diameters in Fig. 4(e). In the experiments, we chose such near-optimal time-delay cases from a multitude of experiments due to the experimental limitations of using a single syringe pump. For practical antibubble generation, we recommend to use a droplet generator [35,36], which can precisely control the droplet generation frequency.

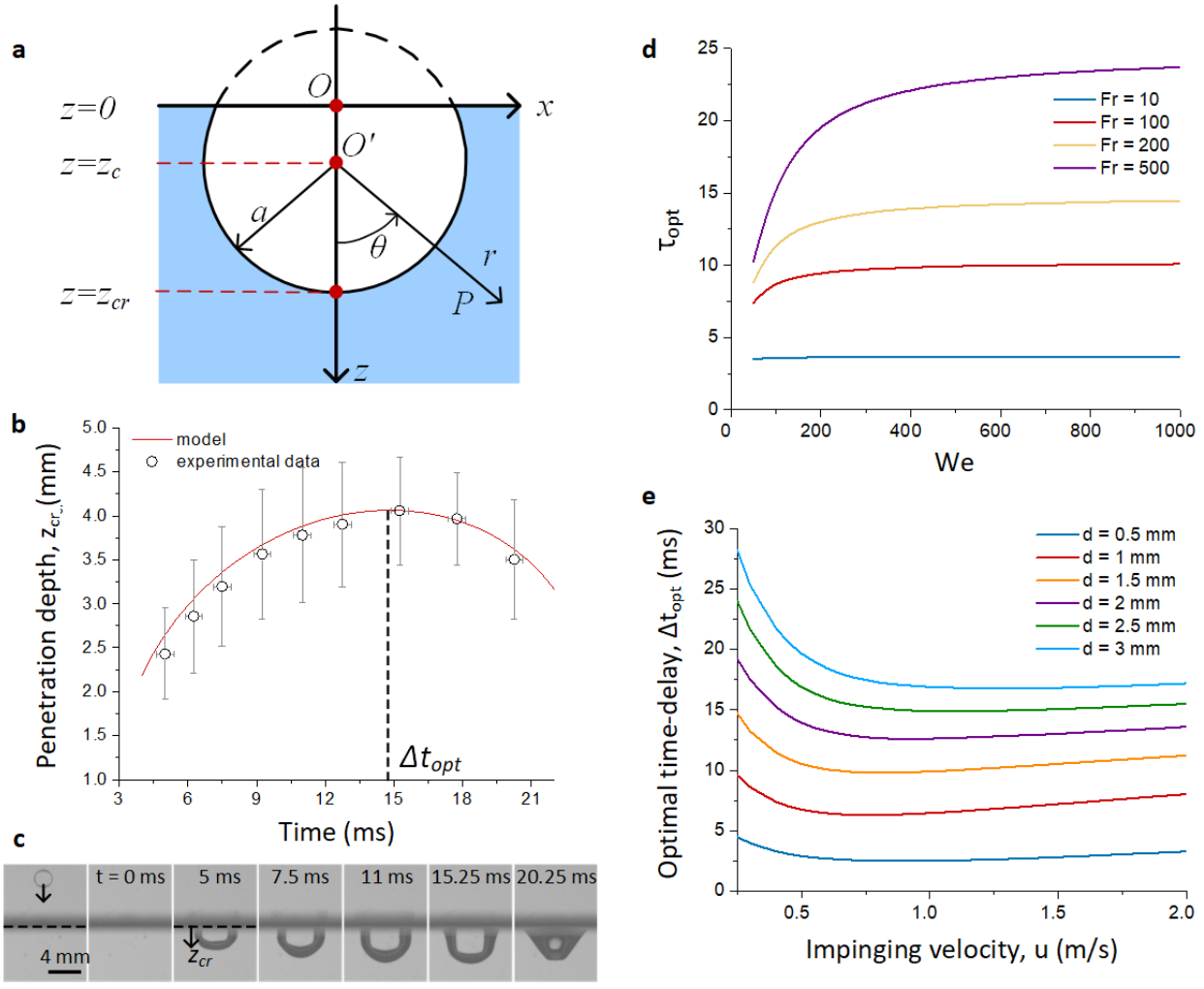

FIG. 4. Crater evolution by the first drop impingement. (a) Schematic of the cavity and notations of moving reference frames. (b) Penetration depth from the equations Error: Reference source not found and Error: Reference source not found as a function of time for the impinging drop with a diameter of 2.48 mm and velocity of 1.24 m/s with corresponding experimental data points (open circles). (c) Time-lapse images of crater evolution from high-speed camera. (d) Dimensionless optimal time-delay as a function of Weber number for different Froude numbers. (e) Optimal time-delay as a function of impinging velocity for different diameters.

C. Energetic analysis

By the successive impact of a following drop on the crater at the optimal time-delay, the increase of the surface energy $\Delta E_\sigma = 4\pi(d/2+\varepsilon)^2\sigma$, where ε is the thickness of the air gap, from stage 1 to stage 4 can result from the total kinetic energy of two drops $E_{K1}+E_{K2}$. Therefore, the energetic criteria for antibubble formation is found from the overall energy balance ($E_{K1}+E_{K2}>\Delta E_\sigma$), which is expressed in terms of the summative Weber number

$$We_{sum} > O(0) \qquad 55\backslash* \text{ MERGEFORMAT ()}$$

where $O(0)$ means the order of magnitude is 0. For convenience, we define the summative Weber number as $We_{sum} = (E_{K1}+E_{K2})/\Delta E_\sigma$. Fig. 5 shows a representative experimental result of two drops impinging at $We_{sum} < 1$. In Fig. 5, the first impinging drop created an initial surface

deformation at 0 ms followed by further surface deformation by the second-drop impingement at 5 ms. However, due to insufficient kinetic energy of the two drops, the second drop could not create large enough deformation for pinch-off, rather, it bounced back and the deformed bulk liquid surface was recovered at 10 ms.

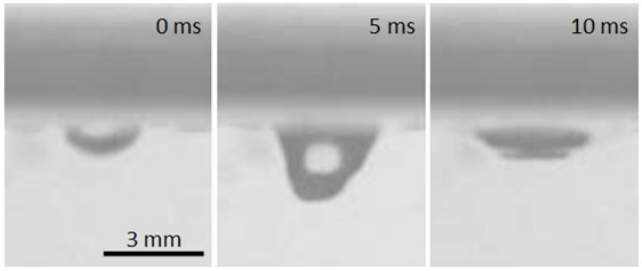

FIG. 5. A representative failure case of antibubble formation due to insufficient total kinetic energy of two impinging drops at $We_{sum} < 1$. An initial surface deformation was created by the first impinging drop at 0 ms. The second drop deformed the surface further at 5 ms. However, due to insufficient kinetic energy of these two drops, the second drop could not penetrate the surface to form an air column, and therefore, the deformed bulk liquid surface was recovered at 10 ms.

D. Pinch-off dynamics

To enable the transition from state 3 to state 4, the pinch-off of the air column should occur before the drainage of air in the gap, from which the third criterion was obtained. Otherwise, the early-drainage of air in the gap leads to the collapse of the air gap as shown in the time-lapse images at 5 ms in Fig. 6(a). For this reason, we compared the characteristic timescale of pinch-off with that of air drainage. Since the Ohnesorge number *Oh* of the drop is on the order of 10^{-3},

the viscous force during the pinch-off process is negligible. Therefore, the pinch-off timescale should be the capillary timescale τ_{cap}, which is deduced from the balance between the inertia and capillary force [14,37,38]

$$\tau_{cap} \sim \sqrt{\rho d^3 / \sigma}. \qquad 66\text{* MERGEFORMAT ()}$$

The drainage timescale τ_{drain} was obtained by analyzing the flow in the air gap between the second drop and the bulk liquid. As shown in Fig. 6(b), the air flow is driven from the bottom to the top of the gap by a pressure drop ΔP, which is composed of the Laplace pressure ΔP_L induced by the curvature of the interface, the hydrostatic pressure ΔP_{hs} due to the presence of gravity, and the stagnation pressure ΔP_{stag} generated by the impinging drop. Specifically, the Laplace pressure difference ΔP_L between the bottom and the top of the drop is scaled as $\Delta P_L \sim \sigma / d \sim 10$ N/m^2. The hydrostatic pressure and the stagnation pressure are scaled as $\Delta P_{hs} \sim \rho g d \sim 10$ N/m^2, and $\Delta P_{stag} = \rho u^2 \sim 10^3$ N/m^2, respectively. Therefore, given the order of magnitude difference, ΔP_{stag} is the dominant source of ΔP, *i.e.*, $\Delta P \sim \Delta P_{stag} \sim \rho u^2$. In addition, considering the ratio of the air gap thickness to the drop diameter, *i.e.*, $\varepsilon / d \sim 10^{-3}$ [10-

12], the air flow through the gap is modeled using the Navier-Stokes equation in spherical coordinates,

$$\frac{\partial P}{\partial \phi} = \frac{\sin\theta}{r}\mu_a \frac{\partial}{\partial r}\left(r^2 \frac{\partial u_\varphi}{\partial r}\right) - \frac{u_\varphi}{r\sin\theta} \quad (77\text{* MERGEFORMAT ()})$$

where θ, ϕ, u_φ are azimuthal angle, polar angle, and the air velocity along the gap, respectively, as shown in Fig. 6(b). By taking $\hat{\phi}$ to be the coordinate along the flow direction and $\hat{r}$ across the gap, the equation Error: Reference source not found can be scaled to yield

$$\rho u^2 \sim \frac{\mu_a u_\varphi R}{\varepsilon^2}. \quad (88\text{* MERGEFORMAT ()})$$

(see Supplemental Material IV for detailed analysis) [20]. By scaling the velocity of air flow as $u_\varphi \sim d/\tau_{drain}$ and substituting it with equation Error: Reference source not found, we can obtain a characteristic timescale of air drainage

$$\tau_{drain} \sim \frac{\mu_a d^2}{\rho u^2 \varepsilon^2}. \quad (99\text{* MERGEFORMAT ()})$$

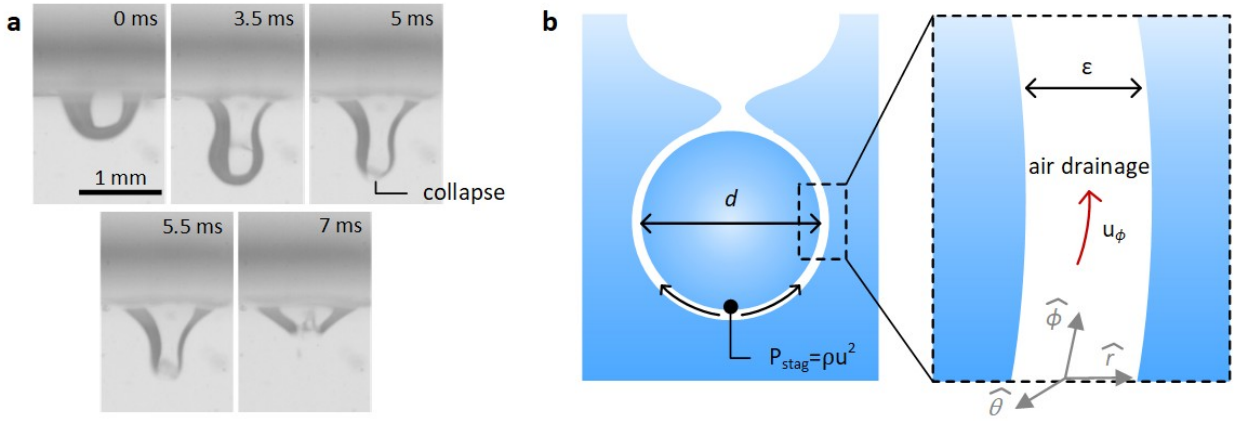

FIG. 6. Experimental images and analysis of a failure case due to early-drainage of air resulting in the collapse of the air gap. (a) Time-lapse experimental images of early-drainage of air. A crater-like initial surface deformation was created by the first impinging drop at 0 ms. The second drop penetrated the deformed surface to form an air column at 3.5 ms. Collapse of the air gap occurred at 5 ms due to the early-drainage of air before pinch-off. The second drop coalesced with the bulk liquid at 5.5 ms and recovered finally at 7 ms. (b) Schematics of an antibubble at the pinch-off step with a magnified view of the air flow within the gap, which is in the ϕ-direction in spherical coordinates.

The diameter d and the impinging velocity u can be directly measured using the high-speed camera. Although a few correlations of air gap thickness ε with antibubble diameter have been reported, they show significant discrepancies with experimental data [11,39]. The experimental measurements showed, on the other hand, that the order of magnitude of the air gap thickness ε is a few micrometers with an average value of ~4 μm [18,39,40]. Therefore, we set ε as a constant value of 4 μm to eliminate the effects of unreliable correlations in the scaling analysis.

Consequently, the ratio of two timescales $\tau_{cap} / \tau_{drain}$ is characterized from the experiments and used as the last criterion for antibubble formation. When $\tau_{cap} / \tau_{drain} < O(0)$, the pinch-off could occur before the drainage of air and the antibubble forms after the pinch-off (Fig. 3). However, if $\tau_{cap} / \tau_{drain} > O(0)$, as shown in Fig. 6(a), air in the gap drains earlier than the pinch-off, leading

to the collapse of the air gap. Note that the ratio of diameters of two drops d_1 / d_2 is also an important parameter for antibubble formation. We determined the ratio of diameters necessary for antibubble formation by considering that the crater created by the first drop needs to accommodate the following drop as well as the no-break-up, no-bouncing, and no-splashing conditions of each drop (see Supplemental Material V for the detailed analysis of the ratio of diameters) [20,41]. To better elucidate the complex energy conversion and dynamic evolution, we maintained the ratio of diameters within $1 < d_1 / d_2 < 2$.

IV. RESULTS

We summarize all four criteria and the corresponding states for antibubble formation by drop pairs in Table 1. As criterion 1 has already been well-understood by single drop dynamics, in this work, we mainly discuss the effect of criteria 2, 3, and 4, which have not been explored in the past. Fig. 7(a) shows the regime map of the antibubble formation with respect to We_{sum} and $\tau_{cap} / \tau_{drain}$ which was obtained from the theoretical prediction and experimental results near the optimal time-delay. Three different regimes were observed, *i.e.*, insufficient surface deformation (marked as blue squares), early-drainage of air (marked as green triangles) and antibubble formation (marked as red circles) (see Supplemental Material for high-speed movies and the size comparison between the diameters of a second drop and an antibubble) [20]. Specifically, the insufficient surface deformation regime occurs when the energetic criterion 2 had not been met, where the surface deformation of the reservoir by the impinging drops was insufficient to form

an air column to be pinched-off later. In this case, bouncing drops were often observed. The experiments also suggest the threshold constant for criterion 2 as $We_{sum} > 3$. The magnified view of the $We_{sum} > 3$ regime (Fig. 7(b)), however, shows the antibubble could not form if the pinch-off was not faster compared to the drainage of air. This result is depicted as the early-drainage of air in the regime map with $\tau_{cap} / \tau_{drain} > O(0)$ and $We_{sum} > 3$. According to the experimental results, a reasonable limit of criterion 4 is $\tau_{cap} / \tau_{drain} < 7$. When $We_{sum} > 3$ and $\tau_{cap} / \tau_{drain} < 7$ were satisfied simultaneously, as expected, a clear regime of antibubble formation was found on the top-left of the regime map (Fig. 7(b)). It is worth pointing out that when $We_{sum} > 3$ and $\tau_{cap} / \tau_{drain} > 7$, both the antibubble and the collapse of the air gap can be observed. We attribute this result to two reasons: a transition (between the early-drainage of air and the antibubble formation regimes) and deviation from the optimal time delay between impingements. First, such transition regimes are commonly found in scaling-based regime maps as the scaling analysis can intrinsically contain uncertainties [19,30,42]. Second, since the actual time-delays were slightly off from the ideal values due to the experimental limitations especially when the drainage process becomes very fast, it can also lead to the mixed regime. To further understand the critical role of the time-delay, we conducted another set of experiments varying the time-delay values while maintaining the $We_{sum} > 3$ and $\tau_{cap} / \tau_{drain} < 7$. We defined the

normalized time-delay difference as $\left(\Delta t - \Delta t_{opt}\right)/\Delta t_{opt}$, where Δt is the measured time-delay. Although all data points are in the regime of antibubble formation with regards to the Weber number and timescale ratio, *i.e.*, $We_{sum} > 3$ and $\tau_{cap} / \tau_{drain} < 7$, antibubbles only form when the normalized time-delay difference is within 30% range (Fig. 7(c, d)) (see Supplemental Material VII, VIII, and IX for the experimental data for time-delay effects, uncertainty analysis, and he experimental data set for antibubble formation, respectively) [20,43]. Therefore, we show that antibubbles can be created in a controllable way following the proposed three criteria.

TABLE I. Criteria of antibubble formation by drop pairs

Criteria	Descriptions	Mechanisms	States
1	$WeOh^{-0.58} > 119$	Cavity formation	2
2	$We_{sum} > 3$	Overall energy conversion	1-4
3	$\Delta t \approx \Delta t_{opt}$	Optimal time-delay between two-drop impacts	2-3
4	$\tau_{cap} / \tau_{drain} < 7$	Pinch-off before air drainage in the gap	3-4

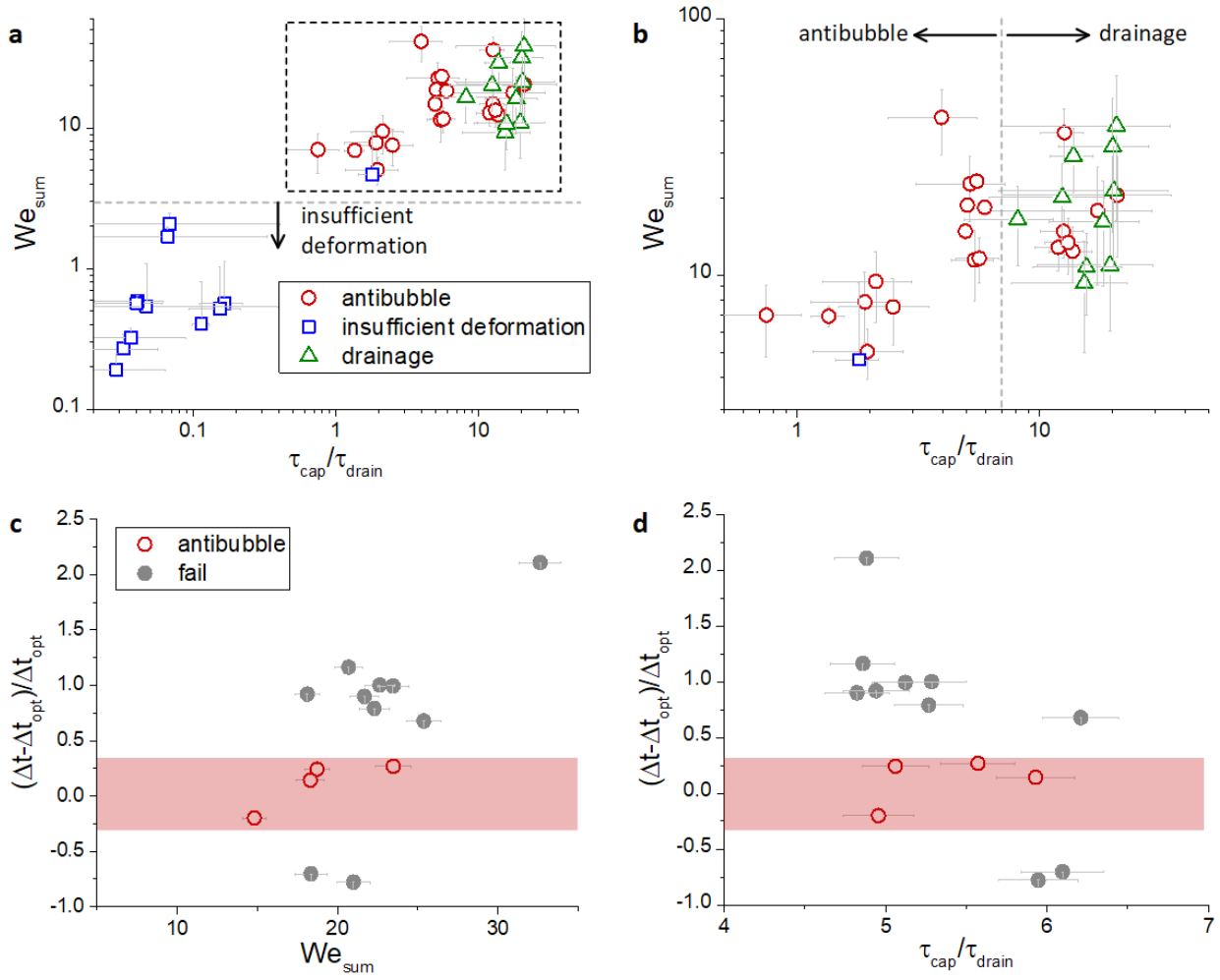

FIG. 7. Experimental results of antibubble formation plotted with the summative Weber number and the ratio of two timescales. Red circles, blue squares, and green triangles represent successful antibubble formation, insufficient deformation of the bulk liquid surface, and failures due to early drainage of air in the gap, respectively. (a) The boundary for summative Weber number is found to be ~3. (b) Magnified view of the dashed box in (a) shows the boundary of the ratio of two timescales is ~7, which shows good agreement with our theoretical analysis. (c, d) The critical role of time-delay between two-drop impingement. Antibubbles only form when the normalized time-delay difference is within 30% range even when criteria for the summative Weber number and the ratio of two timescales are satisfied (shaded in red). The experimental

data for time-delay effects are in Table S1 in Supplemental Material VII. The error bars account for the uncertainties of drop diameter and impinging velocity, which are discussed in Supplemental Material VIII in detail.

V. CONCLUSIONS

In conclusion, four criteria for antibubble formation by drop pairs were proposed based on theoretical analysis and experimental characterizations. In addition to the well-known criterion from single drop impact, two additional dimensionless groups characterized by the summative Weber number We_{sum} and the ratio of air drainage timescale to pinch-off timescale $\tau_{cap} / \tau_{drain}$ were reported, which were obtained by analyzing the overall energy conversion and the air drainage dynamics, respectively. The optimal time-delay condition between two-drop impacts were provided based on the previous literature. A regime map based on theoretical prediction and experimental results were also shown. This study not only offers a physical picture of antibubble formation from drop pairs but also can serve as guidelines for antibubble generation in future studies.

ACKNOWLEDGEMENTS

We appreciate helpful discussion with Prof. John W. M. Bush, Dr. Kyle L. Wilke and Jianyi Du. Y. Song gratefully acknowledges funding received from Exelon Corporation through its membership in the MIT Energy Initiative's Low Carbon Energy Centers. L. Zhang gratefully acknowledges funding support from Singapore-MIT Alliance for Research and Technology (SMART) LEES Program.

REFERENCES

[1] C. L. Stong, The Amateur Scientist: Curious bubbles in which a gas encloses a liquid instead of the other way around, Sci. Am. **230**, 116 (1974).

[2] P. Weiss, The rise of antibubbles: Odd, soggy bubbles finally get some respect, Sci. News **165**, 311 (2004).

[3] W. Hughes and A. R. Hughes, Liquid Drops on the Same Liquid Surface, Nature **129**, 59 (1932).

[4] N. Skogen, Inverted Soap Bubbles—A Surface Phenomenon, Am. J. Phys. **24**, 239 (1956).

[5] M. H. I. Baird, The stability of inverse bubbles, Trans. Faraday Soc. **56**, 213 (1960).

[6] N. V. S. Dorbolo, Antibubbles: evidences of a critical pressure, arXiv:cond-mat/0305126 (2003).

[7] S. Dorbolo, H. Caps, and N. Vandewalle, Fluid instabilities in the birth and death of antibubbles, New J. Phys. **5**, 161 (2003).

[8] J. Zou, C. Ji, B. G. Yuan, X. D. Ruan, and X. Fu, Collapse of an antibubble, Phys. Rev. E **87**, 061002 (2013).

[9] D. N. Sob'yanin, Theory of the Antibubble Collapse, Phys. Rev. Lett. **114**, 104501 (2015).

[10] S. Dorbolo, E. Reyssat, N. Vandewalle, and D. Quéré, Aging of an antibubble, Europhys. Lett. **69**, 966 (2005).

[11] P. G. Kim and J. Vogel, Antibubbles: Factors that affect their stability, Colloids Surf. Physicochem. Eng. Aspects **289**, 237 (2006).

[12] B. Scheid, S. Dorbolo, L. R. Arriaga, and E. Rio, Antibubble Dynamics: The Drainage of an Air Film with Viscous Interfaces, Phys. Rev. Lett. **109**, 264502 (2012).

[13] S. Dorbolo, D. Terwagne, R. Delhalle, J. Dujardin, N. Huet, N. Vandewalle, and N. Denkov, Antibubble lifetime: Influence of the bulk viscosity and of the surface modulus of the mixture, Colloids Surf. Physicochem. Eng. Aspects **365**, 43 (2010).

[14] P. G. Kim and H. A. Stone, Dynamics of the formation of antibubbles, Europhys. Lett. **83**, 54001 (2008).

[15] M. Durand and H. A. Stone, Relaxation Time of the Topological $T1$ Process in a Two-Dimensional Foam, Phys. Rev. Lett. **97**, 226101 (2006).

[16] A. T. Poortinga, Long-Lived Antibubbles: Stable Antibubbles through Pickering Stabilization, Langmuir **27**, 2138 (2011).

[17] S. I. Karakashev and D. S. Ivanova, Thin liquid film drainage: Ionic vs. non-ionic surfactants, J. Colloid Interface Sci. **343**, 584 (2010).

[18] B. Scheid, J. Zawala, and S. Dorbolo, Gas dissolution in antibubble dynamics, Soft Matter **10**, 7096 (2014).

[19] H. Zhao, A. Brunsvold, and S. T. Munkejord, Transition between coalescence and bouncing of droplets on a deep liquid pool, Int. J. Multiphase Flow **37**, 1109 (2011).

[20] See Supplemental Material at [URL] for high-speed movies and information as described in the main text.
[21] A. Prosperetti and H. N. Oguz, The Impact of Drops on Liquid Surfaces and the Underwater Noise of Rain, Annu. Rev. Fluid Mech. **25**, 577 (1993).
[22] M. Rein, Phenomena of liquid drop impact on solid and liquid surfaces, Fluid Dyn. Res. **12**, 61 (1993).
[23] L. J. Leng, Splash formation by spherical drops, J. Fluid Mech. **427**, 73 (2001).
[24] D. Brutin, Drop impingement on a deep liquid surface: study of a crater's sinking dynamics, C. R. Mec. **331**, 61 (2003).
[25] A. I. Fedorchenko and A.-B. Wang, On some common features of drop impact on liquid surfaces, Phys. Fluids **16**, 1349 (2004).
[26] A. Bisighini, G. E. Cossali, C. Tropea, and I. V. Roisman, Crater evolution after the impact of a drop onto a semi-infinite liquid target, Phys. Rev. E **82**, 036319 (2010).
[27] E. Berberović, N. P. van Hinsberg, S. Jakirlić, I. V. Roisman, and C. Tropea, Drop impact onto a liquid layer of finite thickness: Dynamics of the cavity evolution, Phys. Rev. E **79**, 036306 (2009).
[28] A. Bisighini and G. E. Cossali, High-speed visualization of interface phenomena: single and double drop impacts onto a deep liquid layer, J. Visualization **14**, 103 (2011).
[29] H. Ma, C. Liu, X. Li, H. Huang, and J. Dong, Deformation characteristics and energy conversion during droplet impact on a water surface, Phys. Fluids **31**, 062108 (2019).
[30] H. Zhao, A. Brunsvold, and S. T. Munkejord, Investigation of droplets impinging on a deep pool: transition from coalescence to jetting, Exp. Fluids **50**, 621 (2011).
[31] M. V. Gielen *et al.*, Oblique drop impact onto a deep liquid pool, Phys. Rev. Fluids **2**, 083602 (2017).
[32] C. Josserand and S. Zaleski, Droplet splashing on a thin liquid film, Phys. Fluids **15**, 1650 (2003).
[33] E. Castillo-Orozco, A. Davanlou, P. K. Choudhury, and R. Kumar, Droplet impact on deep liquid pools: Rayleigh jet to formation of secondary droplets, Phys. Rev. E **92**, 053022 (2015).
[34] S. T. Thoroddsen, The ejecta sheet generated by the impact of a drop, J. Fluid Mech. **451**, 373 (2002).
[35] H. Ulmke, T. Wriedt, and K. Bauckhage, Piezoelectric Droplet Generator for the Calibration of Particle-Sizing Instruments, Chem. Eng. Technol. **24**, 265 (2001).
[36] B. S. Vaughn, P. J. Tracey, and A. J. Trevitt, Drop-on-demand microdroplet generation: a very stable platform for single-droplet experimentation, RSC Adv. **6**, 60215 (2016).
[37] J. Eggers and E. Villermaux, Physics of liquid jets, Rep. Prog. Phys. **71**, 036601 (2008).
[38] L. Rayleigh, On the capillary phenomena of jets, Proc. R. Soc. London **29**, 71 (1879).
[39] Y. Vitry, S. Dorbolo, J. Vermant, and B. Scheid, Controlling the lifetime of antibubbles, Adv. Colloid Interface Sci. **270**, 73 (2019).
[40] W. Suhr, Gaining insight into antibubbles via frustrated total internal reflection, Eur. J. Phys. **33**, 443 (2012).
[41] Y. Chen *et al.*, in *55th AIAA Aerospace Sciences Meeting* (American Institute of Aeronautics and Astronautics, Grapevine, Texas, USA, 2017).

[42] Y. S. Joung and C. R. Buie, Scaling laws for drop impingement on porous films and papers, Phys. Rev. E **89**, 013015 (2014).
[43] B. N. Taylor and C. E. Kuyatt, (National Institute of Standards and Technology, 1994).